Appl. Math. Mech. -Engl. Ed., **42**(6), 771–786 (2021)

APPLIED MATHEMATICS AND MECHANICS (ENGLISH EDITION)

https://doi.org/10.1007/s10483-021-2725-7

Isogeometric nonlocal strain gradient quasi-three-dimensional plate model for thermal postbuckling of porous functionally graded microplates with central cutout with different shapes*

Rui SONG[1], S. SAHMANI[2], B. SAFAEI[3,†]

1. Department of Civil and Architecture Engineering, Nanchang Institute of Technology, Nanchang 330099, China;
2. Mechanical Rotating Equipment Department, Niroo Research Institute (NRI), Tehran 14665-517, Iran;
3. Department of Mechanical Engineering, Eastern Mediterranean University, Famagusta 99628, North Cyprus via Mersin 10, Turkey

(Received Nov. 24, 2020 / Revised May 1, 2021)

Abstract This study presents the size-dependent nonlinear thermal postbuckling characteristics of a porous functionally graded material (PFGM) microplate with a central cutout with various shapes using isogeometric numerical technique incorporating non-uniform rational B-splines. To construct the proposed non-classical plate model, the nonlocal strain gradient continuum elasticity is adopted on the basis of a hybrid quasi-three-dimensional (3D) plate theory under through-thickness deformation conditions by only four variables. By taking a refined power-law function into account in conjunction with the Touloukian scheme, the temperature-porosity-dependent material properties are extracted. With the aid of the assembled isogeometric-based finite element formulations, nonlocal strain gradient thermal postbuckling curves are acquired for various boundary conditions as well as geometrical and material parameters. It is portrayed that for both size dependency types, by going deeper in the thermal postbuckling domain, gaps among equilibrium curves associated with various small scale parameter values get lower, which indicates that the pronounce of size effects reduces by going deeper in the thermal postbuckling regime. Moreover, we observe that the central cutout effect on the temperature rise associated with the thermal postbuckling behavior in the presence of the effect of strain gradient size and absence of nonlocality is stronger compared with the case including nonlocality in absence of the strain gradient small scale effect.

Key words porosity, functionally graded (FG) composite, isogeometric approach, quasi-three-dimensional (3D) plate theory, nonlocal strain gradient elasticity

Chinese Library Classification O175
2010 Mathematics Subject Classification 83C15, 74D05, 74F05, 74F15

* Citation: SONG, R., SAHMANI, S., and SAFAEI, B. Isogeometric nonlocal strain gradient quasi-three-dimensional plate model for thermal postbuckling of porous functionally graded microplates with central cutout with different shapes. *Applied Mathematics and Mechanics* (*English Edition*), **42**(6), 771–786 (2021) https://doi.org/10.1007/s10483-021-2725-7

† Corresponding author, E-mail: babak.safaei@emu.edu.tr

Project supported by the Natural Science Foundation of Jiangxi Science and Technology Department (No. 20202BAB204027)

1 Introduction

Fabrication of novel composite materials having desired porosity patterns is possible today due to the fantastic advancements in materials science and technology, which can be widely utilized in several fields of industry[1–4]. For example, Jia et al.[5] presented a structure design for a porous nitrogen-doped carbon structure for having an efficient alkaline hydrogen reaction. García-Salaberri[6] introduced a composite continuum-network computational fluid dynamics model to simulate convection diffusion and in anisotropic carbon-paper gas diffusion layers as thin porous media applied in polymer electrolyte fuel cells. Cassio et al.[7] calibrated silicon structure porosities to generate a micro-resonator with well defined refractive indices for biosensors. Xie et al.[8] applied Gurtin-Murdoch theory of elasticity to study nonlinear secondary behavior of functionally graded (FG) porous silicon nanobeams. Hwang et al.[9] fabricated hierarchically porous structured polydimethylsiloxane composites to apply as flexible capacitive pressure sensor having a wide measurement range. Lin et al.[10] proposed an antibacterial and light smart titanium-containing composite with porosity having surfaces with exhibited durably anti-adhesive properties.

For the determination of various small scale effects, they were required to be applied in classical continuum elasticity. Hence, various non-classical continuum elasticity theories were proposed[11–13]. In the past two decades, many research works have been performed to evaluate size-dependent mechanical behaviors of small scaled structures[14–15]. Recently, Fan et al.[16] for the first time proposed for all boundary condition types in axially loaded FG composite microshells frequencies with lower semi-vertex angles, and showed that it was more significant. Yi et al.[17] employed the classical shell theory and the Gurtin-Murdoch surface theory of elasticity to investigate nonlinear large amplitude free vibrations in nanoshell structures. Yang et al.[18] found that, nonlocality size effect reduced critical shortening and critical hydrostatic pressure of FG microshells. Yuan et al.[19] and Fan et al.[20] used surface elasticity theories and nonlocal strain gradient of FG skew nanoplates based on the size-dependent shear buckling behavior theory. Yuan et al.[21–22] explored couple stress-based conical shell models for the analysis of size-dependent nonlinear oscillation and buckling behaviors of FG composite conical microshells. Li et al.[23] studied nonlinear FG composite nanoshell free vibrations based on the Gurtin-Murdoch theory with the modal vibration interaction effect. Qin et al.[24] extended their research works on the nonlinear vibrations of fiber-reinforced composite shells with bolt loosening boundaries. Yang et al.[25] revealed that, increase in material gradient index changed material characteristics from ceramic-rich to metal-rich. Wang et al.[26] evaluated the nonlinear postbuckling behavior of cylindrical nanopanels based on the Gurtin-Murdoch elasticity theory when applying the axial compression and incorporating the size effect. Liu et al.[27] evaluated the biaxial buckling and nonlocal vibrations of double-viscoelastic-functionally graded material (FGM) nanoplates lying on viscoelastic media. Joshi et al.[28] used the strain gradient elasticity to explore temperature effect on the vibrations of cracked Kirchhoff FGM microplates. Radić and Jeremić[29] studied the buckling and vibrations of orthotropic double-layered graphene sheets under hygrothermal loadings based on the differential form of nonlocal theory of elasticity. Al-Shujairi and Mollamahmutoğlu[30] developed a nonlocal strain gradient beam model for the free vibration and buckling responses of FGM sandwich microbeams under thermal conditions. Jamalpoor et al.[31] investigated the biaxial buckling and free oscillations of double magneto-electro-elastic nanoplates in viscoelastic media. Hajmohammad et al.[32] investigated the buckling and bending responses of FGM composite annular microplates with piezoelectric facesheets based on the nonlocal continuum elasticity. Lu et al.[33] used the nonlocal strain gradient theory and the surface theory of elasticity based on Mindlin and Kirchhoff plate models for the analysis of nanoplate dynamic response. Sarafraz et al.[34] developed an analytical mathematical solution for nonlocal strain gradient free vibrational response of post-buckled laminated FGM microbeams. Sobhy and Zenkour[35] investigated inhomogeneity and

porosity effects on the buckling and size-dependent oscillations of FGM composite quasi-three-dimensional (3D) nanoplates. Lu et al.[36] constructed a nonlocal strain gradient shell model considering surface stress effect for the free vibrations of FGM cylindrical nanoshell structures. Lu et al.[37] developed a unified size-dependent plate model by the incorporation of strain gradient, nonlocality, and surface stress size dependencies. Fang et al.[38] developed a novel nonlocal Euler-Bernoulli beam model to study the thermal buckling and vibrations of FGM composite nanobeam structures under thermal conditions.

In the current research, on the basis of a hybrid-type quasi-3D higher-order shear deformation theory (HSDT), the nonlocal strain gradient nonlinear postbuckling of porous functionally graded material (PFGM) microplates with a central cutout and various shapes under thermal loads is evaluated. According to the Touloukian scheme and a refined power-law function, temperature- and porosity-dependent material characteristics are derived. Then, isogeometric numerical solving process incorporating non-uniform rational B-splines is applied to obtain nonlinear nonlocal strain gradient equilibrium paths.

2 Quasi-3D nonlocal strain gradient PFGM plate model

In this investigation, typical rectangular microplates with a central cutout prepared from a PFGM are taken into consideration. For this purpose, three different kinds of porous distribution scheme are supposed as shown schematically in Fig. 1.

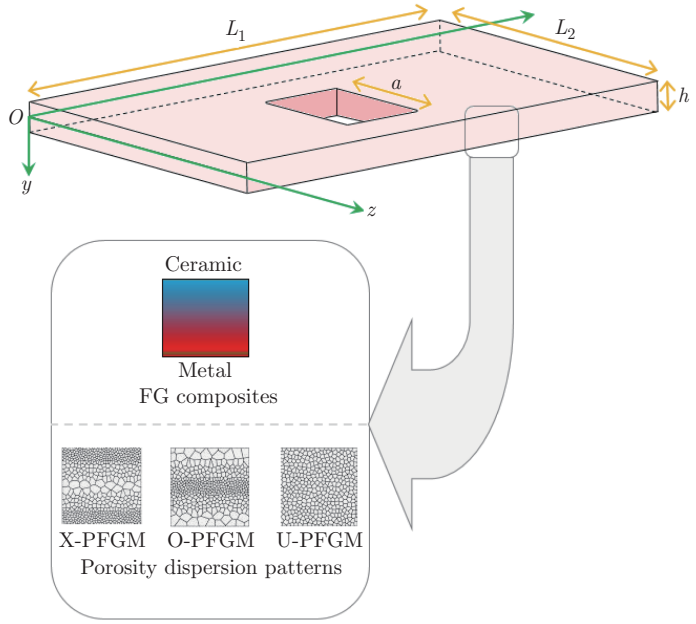

Fig. 1 Porous FGM microplate with central cutout (color online)

Consequently, a porosity-dependent rule of mixture is employed to estimate the material fulfilling the partition of unity in the following form[39]:

$$P(z) = P_{\mathrm{c}}\left(\left(\frac{1}{2}+\frac{z}{h}\right)^{k}-\frac{\Gamma}{2}\right)+P_{\mathrm{m}}\left(1-\left(\frac{1}{2}+\frac{z}{h}\right)k-\frac{\Gamma}{2}\right), \tag{1}$$

in which Γ and k are the porosity and material property gradient indices, respectively. Subscripts c and m denote ceramic and metal, respectively. Consequently, the effective Poisson's

ratio and Young's modulus of PFGM microplates relevant to each kind of the porosity dispersion scheme can be extracted based on the porosity-dependent rule of mixture as

$$E(z) = (E_{\mathrm{c}} - E_{\mathrm{m}})\varphi_1(z) + E_{\mathrm{m}} - (E_{\mathrm{c}} + E_{\mathrm{m}})\Gamma\varphi_2(z), \tag{2a}$$

$$\nu(z) = (\nu_{\mathrm{c}} - \nu_{\mathrm{m}})\varphi_1(z) + E_{\mathrm{m}} - (\nu_{\mathrm{c}} + \nu_{\mathrm{m}})\Gamma\varphi_2(z), \tag{2b}$$

where

$$\varphi_1(z) = \left(\frac{1}{2} + \frac{z}{h}\right)^k, \quad \varphi_2(z) = \begin{cases} \dfrac{1}{2} & \text{for} \quad \text{U-PFGM}, \\ \dfrac{1}{2} - \dfrac{|z|}{h} & \text{for} \quad \text{O-PFGM}, \\ -\dfrac{|z|}{h} & \text{for} \quad \text{X-PFGM}. \end{cases} \tag{3}$$

In Fig. 2, dimensionless effective Young's modulus ($E(z)/E_{\mathrm{c}}$) variations through the thickness of the plate and porosity index of PFGM microplates are plotted for various material property gradient indices.

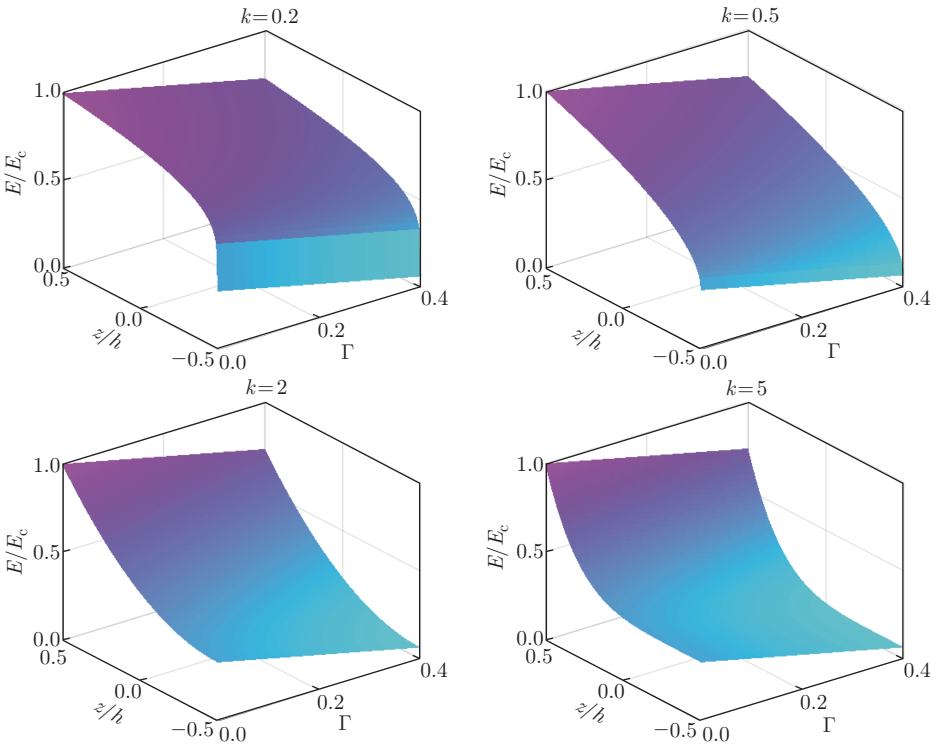

Fig. 2 Variations of Young's modulus for U-PFGM microplate with porosity index and through thickness for various values of material property gradient index (color online)

By establishing a plate theory incorporating higher-order shear deformation expressions, the displacement field is given as

$$U_x(x, y, z) = u(x, y) - zw_{,x}(x, y) + f(z)(\Psi_x(x, y) + w_{,x}(x, y)), \tag{4a}$$

$$U_y(x, y, z) = v(x, y) - zw_{,y}(x, y) + f(z)(\Psi_y(x, y) + w_{,y}(x, y)), \tag{4b}$$

$$U_z(x, y, z) = w(x, y), \tag{4c}$$

in which u, v, and w are mid-plane displacements along x-, y-, and z-axes, and Ψ_x, Ψ_y are rotations about x- and y-axes, respectively. $f(z)$ represents the transverse shear shape function to consider the shear deformation.

By separating the transverse displacement variable into shear and bending components, and implementing transverse normal shape function $g(z)$ to take the normal strains through the thickness into consideration, one has

$$U_x(x,y,z) = u(x,y) - zw_{\mathrm{b},x}(x,y) + (f(z)-z)w_{\mathrm{s},x}(x,y), \tag{5a}$$
$$U_y(x,y,z) = v(x,y) - zw_{\mathrm{b},y} + (f(z)-z)w_{\mathrm{s},y}(x,y), \tag{5b}$$
$$U_z(x,y,z) = w_{\mathrm{b}}(x,y) + (1+g(z))w_{\mathrm{s}}(x,y), \tag{5c}$$

where $w_{\mathrm{b}}(x,y)$ and $w_{\mathrm{s}}(x,y)$ denote, respectively, the bending and shear displacement variables. By assuming a sinusoidal shear function for $f(z)$, and a trigonometric shape function for $g(z)$, the hybrid-type quasi-3D higher-order shear deformation theory can be achieved. Thus, it is supposed that

$$F(z) = f(z) - z = \sin(\pi z/h) - z, \tag{6a}$$
$$G(z) = 1 + g(z) = 1 + 5/(12\pi)\cos(\pi z/h). \tag{6b}$$

Now, strain-displacement equations including the von-Karman geometric nonlinearity can be expressed based on the developed hybrid-type quasi-3D HSDT as follows:

$$\begin{cases} \varepsilon_{xx} = u_{,x} + (w_{\mathrm{b},x} + w_{\mathrm{s},x})^2/2 - zw_{\mathrm{b},xx} + F(z)w_{\mathrm{s},xx}, \\ \varepsilon_{yy} = v_{,y} + (w_{\mathrm{b},y} + w_{\mathrm{s},y})^2/2 - zw_{\mathrm{b},yy} + F(z)w_{\mathrm{s},yy}, \\ \varepsilon_{zz} = G_{,z}(z)w_{\mathrm{s}}, \\ \gamma_{xy} = u_{,y} + v_{,x} + (w_{\mathrm{b},x} + w_{\mathrm{s},x})(w_{\mathrm{b},y} + w_{\mathrm{s},y}) - 2zw_{\mathrm{b},xy} + 2F(z)w_{\mathrm{s},xy}, \\ \gamma_{xz} = (F_{,z}(z) + G(z))w_{\mathrm{s},x}, \\ \gamma_{yz} = (F_{,z}(z) + G(z))w_{\mathrm{s},y}. \end{cases} \tag{7}$$

Accordingly, the stress-strain constitutive equations are stated as

$$\begin{pmatrix} \sigma_{xx} \\ \sigma_{yy} \\ \sigma_{zz} \\ \tau_{xy} \\ \tau_{yz} \\ \tau_{xz} \end{pmatrix} = \begin{pmatrix} Q_{11}(z) & Q_{12}(z) & Q_{13}(z) & 0 & 0 & 0 \\ Q_{12}(z) & Q_{22}(z) & Q_{23}(z) & 0 & 0 & 0 \\ Q_{13}(z) & Q_{23}(z) & Q_{33}(z) & 0 & 0 & 0 \\ 0 & 0 & 0 & Q_{44}(z) & 0 & 0 \\ 0 & 0 & 0 & 0 & Q_{55}(z) & 0 \\ 0 & 0 & 0 & 0 & 0 & Q_{66}(z) \end{pmatrix} \left(\begin{pmatrix} \varepsilon_{xx} \\ \varepsilon_{yy} \\ \varepsilon_{zz} \\ \gamma_{xy} \\ \gamma_{yz} \\ \gamma_{xz} \end{pmatrix} - \begin{pmatrix} \varepsilon_{xx}^{\mathrm{TH}} \\ \varepsilon_{yy}^{\mathrm{TH}} \\ \varepsilon_{zz}^{\mathrm{TH}} \\ 0 \\ 0 \\ 0 \end{pmatrix} \right), \tag{8}$$

where

$$\begin{cases} Q_{11}(z) = Q_{22}(z) = Q_{33}(z) = \dfrac{(1-\nu(z))E(z)}{(1-2\nu(z))(1+\nu(z))}, \\ Q_{12}(z) = Q_{13}(z) = Q_{23}(z) = \dfrac{\nu(z)E(z)}{(1-2\nu(z))(1+\nu(z))}, \\ Q_{44}(z) = Q_{55}(z) = Q_{66}(z) = \dfrac{E(z)}{2(1+\nu(z))}, \\ \varepsilon_{xx}^{\mathrm{TH}} = \varepsilon_{yy}^{\mathrm{TH}} = \varepsilon_{zz}^{\mathrm{TH}} = \alpha(z)\Delta T. \end{cases} \tag{9}$$

Based on the nonlocal strain gradient continuum elasticity, the total stress tensor is expressed as[40]

$$\Phi_{ij} = \sigma_{ij} - \nabla\sigma^*_{ijm}, \tag{10}$$

where the classical and higher-order stresses are given, respectively, as

$$\sigma_{ij} = \int_V \chi_1(x', x, e_1) C_{ijkl}\varepsilon_{kl}\mathrm{d}V, \tag{11a}$$

$$\sigma^*_{ijm} = l^2 \int_V \chi_2(x', x, e_1) C_{ijkl}\varepsilon_{kl}\mathrm{d}V, \tag{11b}$$

in which e_1 and e_2 are nonlocal parameters taking into account the nonlocal stress type of size dependency. Also l indicates strain gradient microstructural size effect. Moreover, the components of strain, strain gradient, and elastic stiffness are represented as ε_{kl}, $\varepsilon_{kl,m}$, and C_{ijkl}, respectively. Based upon the nonlocal strain gradient continuum elasticity, the two kernel functions of $\chi_1(x', x, e_1)$ and $\chi_2(x', x, e_2)$ are supposed to satisfy the corresponding conditions defined by Eringen[41] as

$$\sigma_{ij} - e_1^2(\sigma_{ij,xx} + \sigma_{ij,yy}) = C_{ijkl}\varepsilon_{kl}, \tag{12a}$$

$$\sigma^*_{ijm} - e_2^2(\sigma^*_{ijm,xx} + \sigma^*_{ijm,yy}) = l^2 C_{ijkl}\varepsilon_{kl,m}. \tag{12b}$$

Consequently, the nonlocal strain gradient elasticity-based generalized constitutive equation can be expressed as

$$\begin{aligned}&\Big(1 - e_1^2\Big(\frac{\partial^2}{\partial x^2} + \frac{\partial^2}{\partial y^2}\Big)\Big)\Big(1 - e_1^2\Big(\frac{\partial^2}{\partial x^2} + \frac{\partial^2}{\partial y^2}\Big)\Big)\Phi_{ij}\\ &= \Big(1 - e_1^2\Big(\frac{\partial^2}{\partial x^2} + \frac{\partial^2}{\partial y^2}\Big)\Big)C_{ijkl}\varepsilon_{kl} - l^2\Big(1 - e_2^2\Big(\frac{\partial^2}{\partial x^2} + \frac{\partial^2}{\partial y^2}\Big)\Big)C_{ijkl}\frac{\partial^2\varepsilon_{kl}}{\partial x^2}.\end{aligned} \tag{13}$$

With the assumption of $e_1 = e_2 = e$, one has

$$\Phi_{ij} - e^2(\Phi_{ij,xx} + \Phi_{ij,yy}) = C_{ijkl}\varepsilon_{kl} - l^2 C_{ijkl}(\varepsilon_{kl,xx} + \varepsilon_{kl,yy}). \tag{14}$$

Accordingly, strain energy variations for a PFGM microplate modeled via the nonlocal strain gradient hybrid-type quasi-3D higher-order shear deformation theory can be expressed as

$$\delta\Pi_S = \int_S \int_{-\frac{h}{2}}^{\frac{h}{2}} \Phi_{ij}\delta\varepsilon_{ij}\mathrm{d}z\mathrm{d}S. \tag{15}$$

Based on the principle of virtual work, and through substituting equations (7) and (8) into equation (15), one has

$$\begin{aligned}&\int_S (\delta(P_{\mathrm{b}}^{\mathrm{T}})\xi_{\mathrm{b}}P_{\mathrm{b}} - l^2\delta(\nabla^2 P_{\mathrm{b}}^{\mathrm{T}})\xi_{\mathrm{b}}P_{\mathrm{b}} + \delta(P_{\mathrm{s}}^{\mathrm{T}})\xi_{\mathrm{s}}P_{\mathrm{s}} - l^2\delta(\nabla^2 P_{\mathrm{s}}^{\mathrm{T}})\xi_{\mathrm{s}}P_{\mathrm{s}} - \delta(P_{\mathrm{b}}^{\mathrm{T}})Z^{\mathrm{TH}}\\ &+ l^2\delta(\nabla^2 P_{\mathrm{b}}^{\mathrm{T}})Z^{\mathrm{TH}})\mathrm{d}S = 0,\end{aligned} \tag{16}$$

in which

$$\begin{cases} P_{\mathrm{b}} = \begin{pmatrix} u_{,x} + (w_{\mathrm{b},x} + w_{\mathrm{s},x})^2/2 & -w_{\mathrm{b},xx} & w_{\mathrm{s},xx} & 0 \\ v_{,y} + (w_{\mathrm{b},y} + w_{\mathrm{s},y})^2/2 & -w_{\mathrm{b},xx} & w_{\mathrm{s},yy} & 0 \\ u_{,y} + v_{,x} + (w_{\mathrm{b},x} + w_{\mathrm{s},x})(w_{\mathrm{b},y} + w_{\mathrm{s},y}) & -2w_{\mathrm{b},xy} & 2w_{\mathrm{s},xy} & 0 \\ 0 & 0 & 0 & w_{\mathrm{s}} \end{pmatrix}^{\mathrm{T}}, \\ \xi_{\mathrm{b}} = \begin{pmatrix} A_{\mathrm{b}} & B_{\mathrm{b}} & C_{\mathrm{b}} & E_{\mathrm{b}} \\ B_{\mathrm{b}} & D_{\mathrm{b}} & F_{\mathrm{b}} & G_{\mathrm{b}} \\ C_{\mathrm{b}} & F_{\mathrm{b}} & H_{\mathrm{b}} & K_{\mathrm{b}} \\ E_{\mathrm{b}} & G_{\mathrm{b}} & K_{\mathrm{b}} & J_{\mathrm{b}} \end{pmatrix}, \quad P_{\mathrm{s}} = \begin{pmatrix} w_{\mathrm{s},x} \\ w_{\mathrm{s},y} \end{pmatrix}, \\ Z^{\mathrm{TH}} = \begin{pmatrix} N^{\mathrm{TH}} \\ M_{\mathrm{b}}^{\mathrm{TH}} \\ M_{\mathrm{s}}^{\mathrm{TH}} \\ R^{\mathrm{TH}} \end{pmatrix}, \quad \xi_{\mathrm{s}} = \int_{-\frac{h}{2}}^{\frac{h}{2}} (F_{,z}(z) + G(z))^2 \begin{pmatrix} Q_{44}(z) & 0 \\ 0 & Q_{55}(z) \end{pmatrix} \mathrm{d}z, \end{cases} \tag{17}$$

where

$$\begin{cases} (A_{\mathrm{b}}, B_{\mathrm{b}}, C_{\mathrm{b}}) = \int_{-\frac{h}{2}}^{\frac{h}{2}} (1, z, F(z)) \begin{pmatrix} Q_{11}(z) & Q_{12}(z) & 0 & Q_{13}(z) \\ Q_{12}(z) & Q_{22}(z) & 0 & Q_{23}(z) \\ 0 & 0 & Q_{66}(z) & 0 \\ Q_{31}(z) & Q_{32}(z) & 0 & Q_{33}(z) \end{pmatrix} \mathrm{d}z, \\ (D_{\mathrm{b}}, E_{\mathrm{b}}, F_{\mathrm{b}}, G_{\mathrm{b}}) = \int_{-\frac{h}{2}}^{\frac{h}{2}} \Big(z^2, \frac{\mathrm{d}G(z)}{\mathrm{d}z}, zF(z), z\frac{\mathrm{d}G(z)}{\mathrm{d}z}\Big) \\ \qquad \cdot \begin{pmatrix} Q_{11}(z) & Q_{12}(z) & 0 & Q_{13}(z) \\ Q_{12}(z) & Q_{22}(z) & 0 & Q_{23}(z) \\ 0 & 0 & Q_{66}(z) & 0 \\ Q_{31}(z) & Q_{32}(z) & 0 & Q_{33}(z) \end{pmatrix} \mathrm{d}z, \\ (H_{\mathrm{b}}, K_{\mathrm{b}}, J_{\mathrm{b}}) = \int_{-\frac{h}{2}}^{\frac{h}{2}} \Big(F^2(z), F(z)\frac{\mathrm{d}G(z)}{\mathrm{d}z}, \Big(\frac{\mathrm{d}G(z)}{\mathrm{d}z}\Big)^2\Big) \\ \qquad \cdot \begin{pmatrix} Q_{11}(z) & Q_{12}(z) & 0 & Q_{13}(z) \\ Q_{12}(z) & Q_{22}(z) & 0 & Q_{23}(z) \\ 0 & 0 & Q_{66}(z) & 0 \\ Q_{31}(z) & Q_{32}(z) & 0 & Q_{33}(z) \end{pmatrix} \mathrm{d}z, \\ (N^{\mathrm{TH}}, M_{\mathrm{b}}^{\mathrm{TH}}, M_{\mathrm{s}}^{\mathrm{TH}}, R^{\mathrm{TH}}) = \Delta T \int_{-\frac{h}{2}}^{\frac{h}{2}} \Big(1, z, F(z), \frac{\mathrm{d}G(z)}{\mathrm{d}z}\Big) \\ \qquad \cdot \begin{pmatrix} Q_{11}(z) & Q_{12}(z) & 0 & Q_{13}(z) \\ Q_{12}(z) & Q_{22}(z) & 0 & Q_{23}(z) \\ 0 & 0 & Q_{66}(z) & 0 \\ Q_{31}(z) & Q_{32}(z) & 0 & Q_{33}(z) \end{pmatrix} \alpha(z)\mathrm{d}z. \end{cases} \tag{18}$$

3 Isogeometric solution methodology

Recently, isogeometric numerical solution process has become very popular[42–43]. Within a one-dimensional domain, the non-decreasing form of associated knot vector is expressed as

$$K(\xi) = (\xi_1, \xi_2, \xi_3, \cdots, \xi_{m+n+1}), \tag{19}$$

where m and n in order stand for basis function number and B-spline basis function order. In addition, for each ith knot, $0 \leqslant \xi_i \leqslant 1$ condition has to be satisfied. As a consequence, the

B-spline basis function is written based on the recursive Cox-de Boor equation as follows:

$$X_{i,0}(\xi) = \begin{cases} 1, & \xi_i \leqslant \xi < \xi_{i+1}, \\ 0, & \text{else}, \end{cases} \tag{20a}$$

$$X_{i,n}(\xi) = \frac{\xi - \xi_i}{\xi_{i+n} - \xi_i} X_{i,n-1}(\xi) + \frac{\xi_{i+n+1} - \xi}{\xi_{i+n+1} - \xi_{i+1}} X_{i+1,n-1}(\xi). \tag{20b}$$

In a two-dimensional domain, the tensor product of two basis functions can be utilized to achieve the associated B-spline basis function as follows:

$$\mathcal{F}_{i,j}^{p,q}(\xi,\eta) = \sum_{i=1}^{m} \mathcal{J}_i(x,y) P_i, \tag{21}$$

where P_i denote the control points within the bi-directional control net, and

$$\mathcal{J}_i(\xi,\eta) = \frac{X_{i,p}(\xi) X_{j,q}(\eta) W_{i,j}}{\sum\limits_{i=1}^{m} \sum\limits_{j=1}^{m} X_{i,p}(\xi) X_{j,q}(\eta) W_{i,j}}, \tag{22}$$

in which $X_{i,p}(\xi)$ and $X_{j,q}(\eta)$ represent the shape functions of orders p and q along ξ- and η-directions, respectively. In addition, $W_{i,j}$ is relevant weight coefficient. Thereafter, $K(\eta)$ knot vector is employed to extract shape function $X_{j,q}(\eta)$ derivation. In Fig. 3, the cubic elements considered for square microplates in the presence and absence of a central cutout are shown.

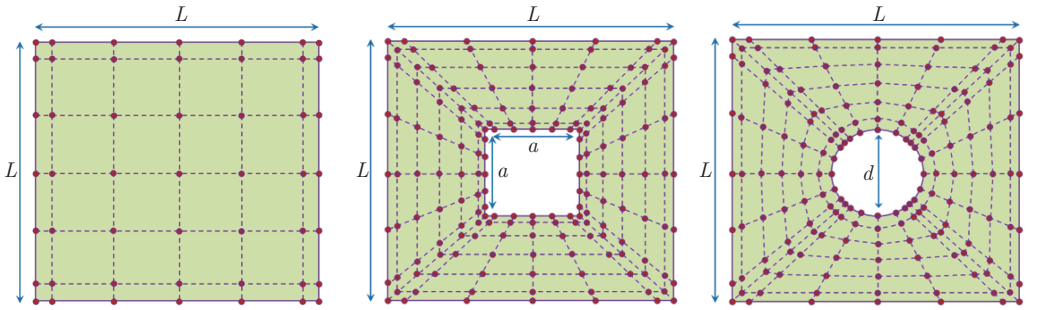

(a) Microplate without central cutout (b) Microplate with square cutout (c) Microplate with circular cutout

Fig. 3 Cubic elements for square microplate structures with geometrical parameters: (a) microplate without central cutout, (b) microplate with square cutout, (c) microplate with circular cutout (color online)

4 Numerical results and discussion

Herein, dimensionless nonlocal strain gradient porosity-dependent thermal postbuckling behaviors of the thermally loaded PFGM microplates with and without a central cutout with different shapes are analyzed. The bottom and top surfaces of PFGM microplates are assumed to be metal-rich and ceramic-rich, respectively. In accordance with the Touloukian scheme, the temperature-dependent of Young's modulus (Pa) and thermal expansion coefficient (K^{-1}) corresponding to each phase can be obtained[44].

Also, one has $\nu_{\mathrm{c}} = 0.24$ for the ceramic phase, $\nu_{\mathrm{m}} = 0.35$ for metal phase[45]. Also, the following geometric parameters are considered $h = 20$ μm, $L_1 = 50h$, and $L_1/L_2 = 1$.

Firstly, the validity of the developed solution method is evaluated. To do so, by neglecting the terms associated with the modified couple stress continuum elasticity, critical temperature

parameter of $\Psi_{\mathrm{TH}} = \alpha \Delta T \times 10^3$ is calculated for simply supported isotropic square plates with different length to thickness ratios, and a comparison is made with the findings of Zhao et al.[46] and Zhang et al.[47]. As shown in Table 1, great agreement is achieved confirming solving process accuracy.

Table 1 Comparison of the critical temperature parameter ($\Psi_{\mathrm{TH}} = \alpha \Delta T \times 10^3$) for simply supported isotropic square plates with different length to thickness ratios

L/h	Zhang et al.[47]	Zhao et al.[46]	Current study
10	11.99	11.83	11.97
20	3.12	3.09	3.12
100	0.13	0.13	0.13

Figures 4 and 5 illustrate the classical and nonlocal strain gradient porosity-dependent equilibrium paths for the thermal postbuckling behavior of temperature-dependent U-PFGM microplates without any central cutout for various nonlocal and strain gradient values, respectively. "CCCC" and "SSSS" denote the fully clamped and the fully simply supported, respectively. By comparing nonlocal strain gradient equilibrium paths with their classical counterparts, we deduced that the strain gradient type of size dependency enhances critical buckling temperature rise, and these patterns become greater for higher strain gradient values. However, the nonlocality acts in an opposite manner reducing thermal buckling stiffness.

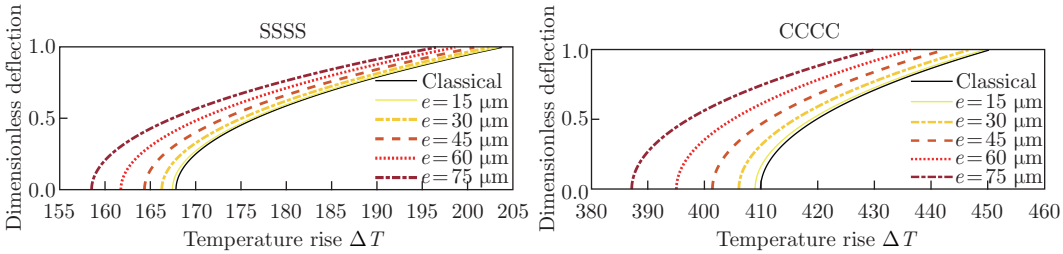

Fig. 4 Dimensionless classical and nonlocal strain gradient nonlinear thermal postbuckling response of U-PFGM microplates for different nonlocal parameter values when $l = 0$ μm, $\Gamma = 0.4$, $k = 0.5$, and $a/L = d/L = 0$ (color online)

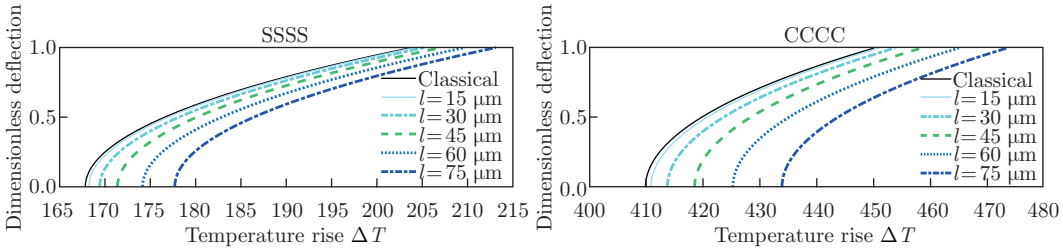

Fig. 5 Dimensionless classical and nonlocal strain gradient nonlinear thermal postbuckling response of U-PFGM microplates for different strain gradient parameter values when $e = 0$ μm, $\Gamma = 0.4$, $k = 0.5$, and $a/L = d/L = 0$ (color online)

Tables 2 and 3 present classical and nonlocal strain gradient temperature rises within the postbuckling regime of temperature-dependent PFGM microplates without any central cutout for various maximum deflections, for various values of material gradient index and nonlocal and strain gradient parameters, respectively. The values given as percentage in parentheses indicate the differences between nonlocal strain gradient temperature rise and its classical counterpart. It is concluded that for a certain maximum plate deflection, temperature rise for O-PFGM porosity dispersion pattern is smaller than that for U-PFGM pattern, and the latter one is

smaller than that obtained for X-PFGM pattern. Also, we witness that for higher material gradient index values, the contributions of both strain gradient size dependency and nonlocality in PFGM microplate thermal postbuckling are intensified. Furthermore, we deduce that for a certain maximum deflection value within thermal postbuckling regime, increase in temperature rise due to strain gradient size effect is more significant than the reduction in corresponding temperature rise due to nonlocality.

The classical and nonlocal strain gradient equilibrium paths for the thermal postbuckling of temperature-dependent PFGM microplates without a central cutout are demonstrated in

Table 2 Classical and nonlocal strain gradient postbuckling temperature rises of PFGM microplates with different porosity dispersion patterns in various material property gradient indices and nonlocal parameters ($\Gamma = 0.4$, $l = 0$ μm)

k	w/h	e/μm	U-PFGM	O-PFGM	X-PFGM
			SSSS boundary conditions		
		0	180.57	168.10	191.28
	0.6	60	179.03 (−0.85%)	166.67 (−0.85%)	189.62 (−0.86%)
0.5		150	171.53 (−5.01%)	159.69 (−5.00%)	181.54 (−5.09%)
		0	220.87	205.65	228.51
	1.2	60	219.67 (−0.54%)	204.53 (−0.53%)	227.14 (−0.60%)
		150	215.88 (−2.26%)	201.02 (−2.23%)	222.06 (−2.82%)
		0	141.23	131.48	149.74
	0.6	60	140.02 (−0.86%)	130.35 (−0.86%)	148.44 (−0.87%)
2		150	134.01 (−5.11%)	124.76 (−5.10%)	141.99 (−5.18%)
		0	169.48	157.80	175.88
	1.2	60	168.42 (−0.62%)	156.81 (−0.61%)	174.71 (−0.67%)
		150	163.91 (−3.28%)	152.64 (−3.23%)	169.48 (−3.64%)
			CCCC boundary conditions		
		0	424.13	394.83	451.46
	0.6	60	420.34 (−0.89%)	391.31 (−0.89%)	447.40 (−0.90%)
0.5		150	401.70 (−5.29%)	373.95 (−5.28%)	427.39 (−5.33%)
		0	469.35	436.97	493.23
	1.2	60	465.94 (−0.73%)	433.79 (−0.72%)	489.49 (−0.76%)
		150	451.46 (−3.81%)	420.33 (−3.78%)	472.86 (−4.13%)
		0	332.97	309.96	354.58
	0.6	60	329.98 (−0.90%)	307.19 (−0.90%)	351.38 (−0.91%)
2		150	315.19 (−5.34%)	293.42 (−5.33%)	335.54 (−5.37%)
		0	364.66	339.50	383.91
	1.2	60	361.85 (−0.77%)	336.88 (−0.76%)	380.86 (−0.80%)
		150	348.74 (−4.37%)	324.70 (−4.32%)	366.38 (−4.56%)

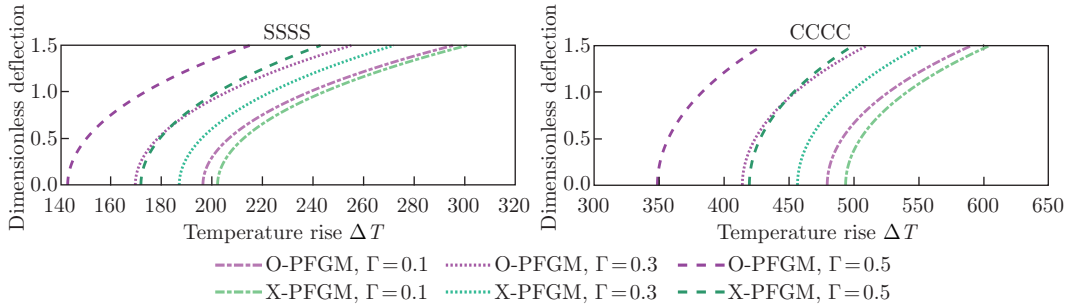

Fig. 6 Dimensionless nonlocal strain gradient nonlinear thermal postbuckling response of PFGM microplates for different porosity indices when $e = l = 60$ μm, $k = 0.5$, and $a/L = d/L = 0$ (color online)

Table 3 Classical and nonlocal strain gradient postbuckling temperature rises of PFGM microplates with different porosity dispersion patterns in various material property gradient indices and strain gradient parameters ($\Gamma = 0.4$, $l = 0$ μm)

k	w/h	e/μm	U-PFGM	O-PFGM	X-PFGM
			SSSS boundary conditions		
0.5	0.6	0	180.57	168.10	191.28
		60	182.13 (+0.86%)	169.55 (+0.86%)	192.95 (+0.87%)
		150	190.35 (+5.42%)	177.21 (+5.41%)	201.76 (+5.48%)
	1.2	0	220.87	205.65	228.51
		60	222.15 (+0.58%)	206.81 (+0.56%)	229.96 (+0.63%)
		150	229.58 (+3.94%)	213.70 (+3.90%)	238.12 (+4.20%)
2	0.6	0	141.23	131.48	149.74
		60	142.47 (+0.87%)	132.63 (+0.87%)	151.06 (+0.88%)
		150	148.96 (+5.47%)	138.67 (+5.46%)	158.01 (+5.52%)
	1.2	0	169.48	157.80	175.88
		60	170.57 (+0.65%)	158.81 (+0.64%)	177.09 (+0.69%)
		150	176.64 (+4.23%)	164.48 (+4.20%)	183.70 (+4.44%)
			CCCC boundary conditions		
0.5	0.6	0	424.13	394.83	451.46
		60	427.96 (+0.91%)	398.40 (+0.90%)	455.56 (+0.92%)
		150	448.12 (+5.65%)	417.17 (+5.63%)	477.12 (+5.69%)
	1.2	0	469.35	436.97	493.23
		60	472.87 (+0.75%)	440.24 (+0.74%)	497.08 (+0.78%)
		150	483.77 (+4.86%)	458.17 (+4.84%)	517.92 (+5.00%)
2	0.6	0	332.97	309.96	354.58
		60	336.01 (+0.92%)	312.79 (+0.92%)	357.82 (+0.93%)
		150	351.90 (+5.69%)	327.60 (+5.68%)	374.85 (+5.73%)
	1.2	0	364.66	339.50	383.91
		60	367.53 (+0.79%)	342.15 (+0.77%)	387.02 (+0.81%)
		150	382.95 (+5.01%)	356.51 (+4.97%)	403.64 (+5.14%)

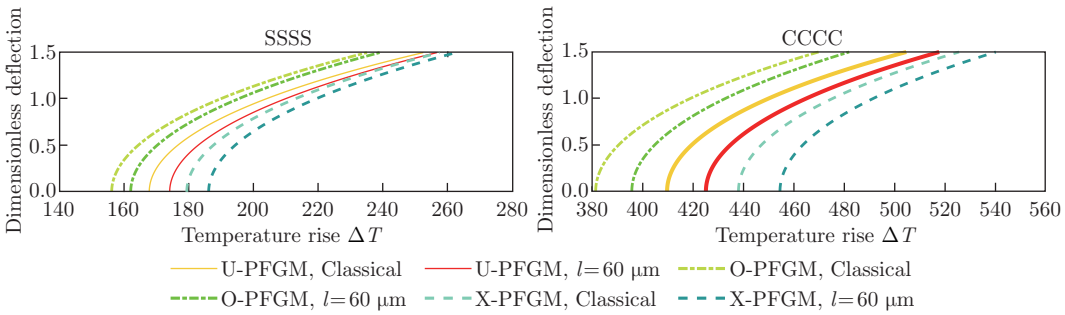

Fig. 7 Dimensionless classical and nonlocal strain gradient nonlinear thermal postbuckling response of PFGM microplates in absence of nonlocal size effect for different porosity dispersion patterns when $e = 0$ μm, $\Gamma = 0.4$, $k = 0.5$, and $a/L = d/L = 0$ (color online)

Figs. 6 and 7 for various values of porosity dispersion pattern and nonlocal and strain gradient parameters, respectively. We concluded that the gap between thermal postbuckling equilibrium paths for different porosity dispersion patterns becomes a bit higher under strain gradient size effect and in the absence of nonlocality. However, by considering nonlocality and ignoring strain gradient size dependency, the gap gets lower.

In order to represent the effect of an existing central cutout on nonlocal strain gradient thermal postbuckling characteristics of microplates, the temperature rise associated with different maximum deflections within the postbuckling regime and various small scale parameters are

Table 4 Influence of the central cutout on the nonlocal strain gradient postbuckling temperature rises of U-PFGM microplates with SSSS boundary conditions ($k = 0.5$, $\Gamma = 0.4$)

e, l/μm	w/h	a/L	ΔT	d/L	ΔT
		0	165.64	0	165.64
		0.1	147.15 (−11.16%)	0.1	154.08 (−6.97%)
	0.5	0.2	140.92 (−14.92%)	0.2	147.86 (−10.73%)
		0.3	131.92 (−20.36%)	0.3	138.86 (−16.17%)
$e = 150$ μm,		0	195.88	0	195.88
$l = 0$ μm		0.1	183.74 (−6.20%)	0.1	187.66 (−4.19%)
	1	0.2	182.96 (−6.59%)	0.2	186.87 (−4.60%)
		0.3	180.61 (−7.79%)	0.3	184.53 (−5.78%)
		0	257.68	0	257.68
		0.1	258.51 (+0.32%)	0.1	256.25 (−0.55%)
	1.5	0.2	268.85 (+4.34%)	0.2	266.69 (+3.46%)
		0.3	280.10 (+8.70%)	0.3	277.84 (+7.82%)
		0	188.46	0	188.46
		0.1	166.92 (−11.43%)	0.1	175.03 (−7.12%)
	0.5	0.2	159.50 (−15.37%)	0.2	167.61 (−11.06%)
		0.3	148.83 (−21.03%)	0.3	156.94 (−16.72%)
$e = 0$ μm,		0	215.10	0	215.10
$l = 150$ μm		0.1	199.15 (−7.41%)	0.1	204.61 (−4.88%)
	1	0.2	196.53 (−8.63%)	0.2	201.98 (−6.10%)
		0.3	191.72 (−10.87%)	0.3	197.17 (−8.33%)
		0	261.27	0	261.27
		0.1	255.02 (−2.39%)	0.1	255.85 (−2.07%)
	1.5	0.2	260.70 (−0.22%)	0.2	261.54 (+0.10%)
		0.3	266.05 (+1.83%)	0.3	266.89 (+2.15%)

Table 5 Influence of the central cutout on the nonlocal strain gradient postbuckling temperature rises of U-PFGM microplates with CCCC boundary conditions ($k = 0.5$, $\Gamma = 0.4$)

e, l/μm	w/h	a/L	ΔT	d/L	ΔT
		0	392.68	0	392.68
		0.1	345.04 (−12.13%)	0.1	363.17 (−7.51%)
	0.5	0.2	327.72 (−16.54%)	0.2	345.85 (−11.93%)
		0.3	303.14 (−22.80%)	0.3	321.27 (−18.18%)
$e = 150$ μm,		0	426.62	0	426.62
$l = 0$ μm		0.1	386.11 (−9.49%)	0.1	400.84 (−6.04%)
	1	0.2	374.89 (−12.12%)	0.2	389.61 (−8.67%)
		0.3	357.78 (−16.14%)	0.3	372.51 (−12.68%)
		0	495.95	0	495.95
		0.1	470.00 (−5.23%)	0.1	477.80 (−3.66%)
	1.5	0.2	471.26 (−4.98%)	0.2	479.06 (−3.40%)
		0.3	469.40 (−5.35%)	0.3	477.20 (−3.78%)
		0	448.72	0	448.72
		0.1	393.71 (−12.26%)	0.1	414.68 (−7.58%)
	0.5	0.2	373.52 (−16.76%)	0.2	394.49 (−12.09%)
		0.3	344.94 (−23.13%)	0.3	365.91 (−18.45%)
$e = 0$ μm,		0	478.62	0	478.62
$l = 150$ μm		0.1	429.88 (−10.18%)	0.1	447.86 (−6.42%)
	1	0.2	415.07 (−13.28%)	0.2	433.04 (−9.52%)
		0.3	393.06 (−17.87%)	0.3	411.05 (−14.12%)
		0	530.42	0	530.42
		0.1	492.56 (−7.14%)	0.1	505.36 (−4.72%)
	1.5	0.2	487.07 (−8.17%)	0.2	499.88 (−5.76%)
		0.3	476.47 (−10.17%)	0.3	489.27 (−7.78%)

tabulated in Tables 4 and 5, corresponding to SSSS and CCCC edge supports, respectively. The value given as percentage in the parentheses indicates differences between temperature rises with and without a central cutout. As can be seen, by assuming higher maximum deflection values (deeper regions of postbuckling domain), the trend is changed specially for a bigger central cutout. Also, it is found that the reduction of PFGM microplate thermal postbuckling strength caused by a square central cutout is more than that of a circular one. Moreover, the central cutout effect on temperature rise associated with the thermal postbuckling behavior in the presence of strain gradient size effect and in the absence of nonlocality is stronger than the case including nonlocality in absence of strain gradient size dependency.

5 Conclusions

The aim of the current investigation is to evaluate the porosity-dependent nonlinear thermal postbuckling behavior of porous FGM microplates under microstructural strain gradient size dependency and stress-driven nonlocal size effect. To this end, non-uniform rational B-splines based isogeometric solution methodology is used together with the Touloukian scheme and the refined power-law function. It was witnessed that the thermal postbuckling strength of the microplate reduces with the increase in material property gradient index value which results in a lower critical temperature rise as well as a higher associated deflection. Also, it is seen that load-deflection variation slope gets lower by moving from the ceramic-rich to metal-rich microplate. In addition, it was shown that at a certain maximum deflection value within the thermal postbuckling regime, the increase of associated temperature rise due to strain gradient size effect is more significant than the reduction in that due to nonlocality.

References

[1] SAHMANI, S. and SAFAEI, B. Large-amplitude oscillations of composite conical nanoshells with in-plane heterogeneity including surface stress effect. *Applied Mathematical Modelling*, **89**, 1792–1813 (2021)

[2] FAN, F., XU, Y., SAHMANI, S., and SAFAEI, B. Modified couple stress-based geometrically nonlinear oscillations of porous functionally graded microplates using NURBS-based isogeometric approach. *Computer Methods in Applied Mechanics and Engineering*, **372**, 113400 (2020)

[3] SAFAEI, B. The effect of embedding a porous core on the free vibration behavior of laminated composite plates. *Steel and Composite Structures*, **35**(5), 659–670 (2020)

[4] YUAN, Y., ZHAO, X., ZHAO, Y., SAHMANI, S., and SAFAEI, B. Dynamic stability of nonlocal strain gradient FGM truncated conical microshells integrated with magnetostrictive facesheets resting on a nonlinear viscoelastic foundation. *Thin-Walled Structures*, **159**, 107249 (2021)

[5] JIA, L., LIU, B., ZHAO, Y., CHEN, W., MOU, D., FU, J., WANG, Y., XIN, W., and ZHAO, L. Structure design of MoS2@Mo2C on nitrogen-doped carbon for enhanced alkaline hydrogen evolution reaction. *Journal of Materials Science*, **55**(34), 16197–16210 (2020)

[6] GARCÍA-SALABERRI, P. A. Modeling diffusion and convection in thin porous transport layers using a composite continuum-network model: application to gas diffusion layers in polymer electrolyte fuel cells. *International Journal of Heat and Mass Transfer*, **167**, 120824 (2021)

[7] CASSIO, F., LORRAIN, N., PIRASTEH, P., POFFO, L., LEMAITRE, J., HARDY, I., and GUENDOUZ, M. Porosity calibration in a 4-layer porous silicon structure to fabricate a microresonator with well-defined refractive indices and dedicated to biosensing applications. *Optical Materials*, **110**, 110468 (2020)

[8] XIE, B., SAHMANI, S., SAFAEI, B., and XU, B. Nonlinear secondary resonance of FG porous silicon nanobeams under periodic hard excitations based on surface elasticity theory. *Engineering with Computers*, 1–24 (2020)

[9] HWANG, J., KIM, Y., YANG, H., and OH, J. H. Fabrication of hierarchically porous structured PDMS composites and their application as a flexible capacitive pressure sensor. *Composites Part B: Engineering*, 108607 (2021)

[10] LIN, J., HU, J., WANG, W., LIU, K., ZHOU, C., LIU, Z., KONG, S., LIN, S., DENG, Y., and GUO, Z. Thermo and light-responsive strategies of smart titanium-containing composite material surface for enhancing bacterially anti-adhesive property. *Chemical Engineering Journal*, **407**, 125783 (2021)

[11] AREFI, M., MOHAMMAD-REZAEI BIDGOLI, E., DIMITRI, R., and TORNABENE, F. Free vibrations of functionally graded polymer composite nanoplates reinforced with graphene nanoplatelets. *Aerospace Science and Technology*, **81**, 108–117 (2018)

[12] SAHMANI, S., AGHDAM, M. M., and RABCZUK, T. Nonlinear bending of functionally graded porous micro/nano-beams reinforced with graphene platelets based upon nonlocal strain gradient theory. *Composite Structures*, **186**, 68–78 (2018)

[13] SAHMANI, S., AGHDAM, M. M., and RABCZUK, T. Nonlocal strain gradient plate model for nonlinear large-amplitude vibrations of functionally graded porous micro/nano-plates reinforced with GPLs. *Composite Structures*, **198**, 51–62 (2018)

[14] TOGUN, N. and BAĞDATLI, S. M. Size dependent nonlinear vibration of the tensioned nanobeam based on the modified couple stress theory. *Composites Part B: Engineering*, **97**, 255–262 (2016)

[15] SAHMANI, S. and SAFAEI, B. Influence of homogenization models on size-dependent nonlinear bending and postbuckling of bi-directional functionally graded micro/nano-beams. *Applied Mathematical Modelling*, **82**, 336–358 (2020)

[16] FAN, L., SAHMANI, S., and SAFAEI, B. Couple stress-based dynamic stability analysis of functionally graded composite truncated conical microshells with magnetostrictive facesheets embedded within nonlinear viscoelastic foundations. *Engineering with Computers* (2020) https://doi.org/10.1007/s00366-020-01182-w

[17] YI, H., SAHMANI, S., and SAFAEI, B. On size-dependent large-amplitude free oscillations of FGPM nanoshells incorporating vibrational mode interactions. *Archives of Civil and Mechanical Engineering*, **20**(2), 48 (2020)

[18] YANG, X., SAHMANI, S., and SAFAEI, B. Postbuckling analysis of hydrostatic pressurized FGM microsized shells including strain gradient and stress-driven nonlocal effects. *Engineering with Computers* (2020) https://doi.org/10.1007/s00366-019-00901-2

[19] YUAN, Y., ZHAO, K., SAHMANI, S., and SAFAEI, B. Size-dependent shear buckling response of FGM skew nanoplates modeled via different homogenization schemes. *Applied Mathematics and Mechanics* (*English Edition*), **41**(4), 587–604 (2020) https://doi.org/10.1007/s10483-020-2600-6

[20] FAN, F., ZHAO, K., SAHMANI, S., and SAFAEI, B. Nonlinear oscillations of composite conical microshells with in-plane heterogeneity based upon a couple stress-based shell model. *Thin-Walled Structures*, **154**, 106841 (2020)

[21] YUAN, Y., ZHAO, K., HAN, Y., SAHMANI, S., and SAFAEI, B. Nonlinear oscillations of composite conical microshells with in-plane heterogeneity based upon a couple stress-based shell model. *Thin-Walled Structures*, **154**, 106857 (2020)

[22] YUAN, Y., ZHAO, K., ZHAO, Y., SAHMANI, S., and SAFAEI, B. Couple stress-based nonlinear buckling analysis of hydrostatic pressurized functionally graded composite conical microshells. *Mechanics of Materials*, **148**, 103507 (2020)

[23] LI, Q., XIE, B., SAHMANI, S., and SAFAEI, B. Surface stress effect on the nonlinear free vibrations of functionally graded composite nanoshells in the presence of modal interaction. *Journal of the Brazilian Society of Mechanical Sciences and Engineering*, **42**(5), 237 (2020)

[24] LI, H., LV, H., SUN, H., QIN, Z., XIONG, J., HAN, Q., LIU, J., and WANG, X. Nonlinear vibrations of fiber-reinforced composite cylindrical shells with bolt loosening boundary conditions. *Journal of Sound and Vibration*, **496**(31), 115935 (2021)

[25] YANG, Y., SAHMANI, S., and SAFAEI, B. Couple stress-based nonlinear primary resonant dynamics of FGM composite truncated conical microshells integrated with magnetostrictive layers. *Applied Mathematics and Mechanics* (*English Edition*), **42**(2), 209–222 (2021) https://doi.org/10.1007/s10483-021-2704-6

[26] WANG, X., ZHOU, G., SAFAEI, B., and SAHMANI, S. Boundary layer modeling of surface residual tension in postbuckling behavior of axially loaded silicon panels at nanoscale embedded in elastic foundations. *Mechanics Based Design of Structures and Machines* (2020) https://doi.org/10.1080/15397734.2020.1794889

[27] LIU, J. C., ZHANG, Y. Q., and FAN, L. F. Nonlocal vibration and biaxial buckling of double-viscoelastic-FGM-nanoplate system with viscoelastic Pasternak medium in between. *Physics Letters, Section A*: *General, Atomic and Solid State Physics*, **381**(14), 1228–1235 (2017)

[28] JOSHI, P. V., GUPTA, A., JAIN, N. K., SALHOTRA, R., RAWANI, A. M., and RAMTEKKAR, G. D. Effect of thermal environment on free vibration and buckling of partially cracked isotropic and FGM micro plates based on a non classical Kirchhoff's plate theory: an analytical approach. *International Journal of Mechanical Sciences*, **131-132**, 155–170 (2017)

[29] RADIĆ, N. and JEREMIĆ, D. A comprehensive study on vibration and buckling of orthotropic double-layered graphene sheets under hygrothermal loading with different boundary conditions. *Composites Part B*: *Engineering*, **128**, 182–199 (2017)

[30] AL-SHUJAIRI, M. and MOLLAMAHMUTOĞLU, Ç. Buckling and free vibration analysis of functionally graded sandwich micro-beams resting on elastic foundation by using nonlocal strain gradient theory in conjunction with higher order shear theories under thermal effect. *Composites Part B*: *Engineering*, **154**, 292–312 (2018)

[31] JAMALPOOR, A., AHMADI-SAVADKOOHI, A., HOSSEINI, M., and HOSSEINI-HASHEMI, S. Free vibration and biaxial buckling analysis of double magneto-electro-elastic nanoplate-systems coupled by a visco-Pasternak medium via nonlocal elasticity theory. *European Journal of Mechanics*, *A/Solids*, **63**, 84–98 (2017)

[32] HAJMOHAMMAD, M. H., ZAREI, M. S., SEPEHR, M., and ABTAHI, N. Bending and buckling analysis of functionally graded annular microplate integrated with piezoelectric layers based on layerwise theory using DQM. *Aerospace Science and Technology*, **79**, 679–688 (2018)

[33] LU, L., GUO, X., and ZHAO, J. On the mechanics of Kirchhoff and Mindlin plates incorporating surface energy. *International Journal of Engineering Science*, **124**, 24–40 (2018)

[34] SARAFRAZ, A., SAHMANI, S., and AGHDAM, M. M. Nonlinear secondary resonance of nanobeams under subharmonic and superharmonic excitations including surface free energy effects. *Applied Mathematical Modelling*, **66**, 195–226 (2019)

[35] SOBHY, M. and ZENKOUR, A. M. Porosity and inhomogeneity effects on the buckling and vibration of double-FGM nanoplates via a quasi-3D refined theory. *Composite Structures*, **220**, 289–303 (2019)

[36] LU, L., ZHU, L., GUO, X., ZHAO, J., and LIU, G. A nonlocal strain gradient shell model incorporating surface effects for vibration analysis of functionally graded cylindrical nanoshells. *Applied Mathematics and Mechanics* (*English Edition*), **40**(12), 1695–1722 (2019) https://doi.org/10.1007/s10483-019-2549-7

[37] LU, L., GUO, X., and ZHAO, J. A unified size-dependent plate model based on nonlocal strain gradient theory including surface effects. *Applied Mathematical Modelling*, **68**, 583–602 (2019)

[38] FANG, J., ZHENG, S., XIAO, J., and ZHANG, X. Vibration and thermal buckling analysis of rotating nonlocal functionally graded nanobeams in thermal environment. *Aerospace Science and Technology*, **106**, 106146 (2020)

[39] PHUNG-VAN, P., THAI, C. H., NGUYEN-XUAN, H., and ABDEL-WAHAB, M. An isogeometric approach of static and free vibration analyses for porous FG nanoplates. *European Journal of Mechanics*, *A/Solids*, **78**, 103851 (2019)

[40] LIM, C. W., ZHANG, G., and REDDY, J. N. A higher-order nonlocal elasticity and strain gradient theory and its applications in wave propagation. *Journal of the Mechanics and Physics of Solids*, **78**, 298–313 (2015)

[41] ERINGEN, A. C. Linear theory of nonlocal elasticity and dispersion of plane waves. *International Journal of Engineering Science*, **10**(5), 425–435 (1972)

[42] FAN, F., SAFAEI, B., and SAHMANI, S. Buckling and postbuckling response of nonlocal strain gradient porous functionally graded micro/nano-plates via NURBS-based isogeometric analysis. *Thin-Walled Structures*, **159**, 107231 (2021)

[43] FAN, F., SAHMANI, S., and SAFAEI, B. Isogeometric nonlinear oscillations of nonlocal strain gradient PFGM micro/nano-plates via NURBS-based formulation. *Composite Structures*, **255**, 112969 (2021)

[44] SHEN, H. S. Thermal postbuckling of shear deformable FGM cylindrical shells with temperature-dependent properties. *Mechanics of Advanced Materials and Structures*, **14**(6), 439–452 (2007)

[45] MILLER, R. E. and SHENOY, V. B. Size-dependent elastic properties of nanosized structural elements. *Nanotechnology*, **11**(3), 139–147 (2000)

[46] ZHAO, X., LEE, Y. Y., and LIEW, K. M. Mechanical and thermal buckling analysis of functionally graded plates. *Composite Structures*, **90**(2), 161–171 (2009)

[47] ZHANG, L. W., ZHU, P., and LIEW, K. M. Thermal buckling of functionally graded plates using a local Kriging meshless method. *Composite Structures*, **108**(1), 472–492 (2014)